



Synthesis, electrochemical and photoluminescence properties of titanium nitride nanoparticles

Xiaoqing Kan¹ · Chengji Deng¹ · Chao Yu¹ · Jun Ding¹ · Hongxi Zhu¹

Received: 3 April 2018 / Accepted: 17 April 2018 / Published online: 28 April 2018
© Springer Science+Business Media, LLC, part of Springer Nature 2018

Abstract

Titanium nitride nanoparticles were efficiently synthesized by molten-salt method in MgCl₂–NaCl media at a low temperature of 700 °C for 1 h, using titanium dioxide and Mg as raw materials in a N₂ atmosphere. The investigations of nanostructure analysis indicate that the as-prepared titanium nitride is a pure phase, and has excellent crystallinity and high Brunauer–Emmett–Teller surface area. Electrochemical tests show that the titanium nitride nanoparticles exhibit a specific capacitance of 26.4 F/g at 0.25 A/g discharge current density and a low internal resistance (R_s) of 2.0 Ω. The photoluminescence spectrum shows four prominent and high intense peaks centered at 279, 420, 561 and 838 nm, suggesting the good optical property of the titanium nitride nanoparticles.

1 Introduction

Titanium nitride (TiN) has attracted considerable attention from researchers due to its excellent properties such as high melting point, extreme hardness, good adhesion to the substrate, excellent corrosion resistance, good electrical conductivity and favorable optical properties [1–6]. In recent years, TiN materials have been exploited systematically in applications for catalyst supports [7], additive [8], energy-saving coatings [9], photocatalytic applications [10], supercapacitors [11], electrode materials [12] and so on.

There are several methods employed for the synthesis of TiN nanoparticles, including carbothermal reduction nitridation [13], self-propagating high-temperature synthesis [14], a sol–gel method [15], low-temperature and solvent-free synthesis [16], and chemical vapor deposition [17]. However, some of these methods have a complex reaction process that is expensive and somewhat unfriendly to the environment. In addition to the above techniques, molten salt synthesis (MSS) has been reported to be one of the most low-temperature and cost-effective means to prepare nitride powders and ceramic materials [18–29].

In this study, the TiN nanoparticles were synthesized by MSS at 700 °C for 1 h, using titanium dioxide (TiO₂) and Mg as raw materials in MgCl₂–NaCl media in a N₂ atmosphere. In addition, the electrochemical and photoluminescence properties of the TiN nanoparticles were revealed.

2 Experimental procedure

TiN nanoparticles were obtained by using powders of TiO₂ (99.0% in purity) and Mg (99.5% in purity) at a 1:2.5 mol ratio as the raw materials. MgCl₂·6H₂O (99.0% in purity) and NaCl (99.5% in purity) at a 1:4 mol ratio were used as the reaction medium. The raw materials and two kinds of salts were mechanically mixed at a weight ratio of 1:1.2 in an alumina crucible and then heated at the temperature of 700 °C for 1 h in a N₂ atmosphere. After cooling down to room temperature, the reacted mass was wash by hydrochloric acid solution (0.5 mol/L) and distilled water to remove the by-products and the residual salt. The final samples were then oven-dried at 110 °C for 12 h prior to further characterizations.

Phase analysis about the product was made by powder X-ray diffraction (XRD, Philips, X'Pert Pro) using Cu Kα radiation. The morphology of the nanostructure was determined by high-resolution transmission electron microscopy (HRTEM, JEOL, JEM2000F) equipped with an energy dispersive X-ray spectroscopy (EDS). The X-ray photoelectron spectra (XPS) were conducted on a VG Multi lab 2000 spectrometer (Thermo

✉ Jun Ding
dingjun@wust.edu.cn

¹ The State Key Laboratory of Refractories and Metallurgy, Wuhan University of Science and Technology, Wuhan 430081, People's Republic of China

Electron Corporation) with Al K α radiation ($h\nu = 1486.6$ eV) as the incident X-ray. A Brunauer–Emmett–Teller (BET) specific-surface-area analysis was conducted to characterize the powders using a fully automatic surface area and porosity analyzer (Quantachrome, Autosorb-1-MP). The electrochemical performance of the material was analyzed on an electrochemical workstation (CHI 760E, Shanghai, China). Photoluminescence (PL) spectra were detected by a fluorescence spectrophotometer (Jobin Yvon, FL3-32, French) at room temperature.

3 Results and discussion

3.1 Crystal structure

Figure 1 shows the XRD pattern of the as-obtained sample. The five intense diffraction peaks at a 2θ of 36.850° , 42.822° , 62.173° , 74.365° , and 78.265° can be readily indexed as the cubic cell of TiN [(111), (200), (220), (311), and (222)], which indicate the high crystallinity and purity of TiN. The reference interplanar distances of the TiN phase (JCPDS file no. 38-1420) in comparison with XRD result are shown in Table 1. The values of interplanar distances for the as-prepared TiN differ from the JCPDS file no. 38-1420 data no more than 0.02 Å. The lattice constant for TiN nanoparticles has been determined to be $a = 4.22$ Å, which is consistent with the literature value (JCPDS file no. 38-1420). The crystallite size of the TiN nanoparticle is calculated to be 27 nm using the Debye–Scherrer relationship [30].

$$D = 0.9\lambda / (\beta \cos \theta)$$

where D denotes the crystallite size (nm); β denotes the full width at half-maximum; λ denotes the incident X-ray wavelength and θ denotes the diffraction angle.

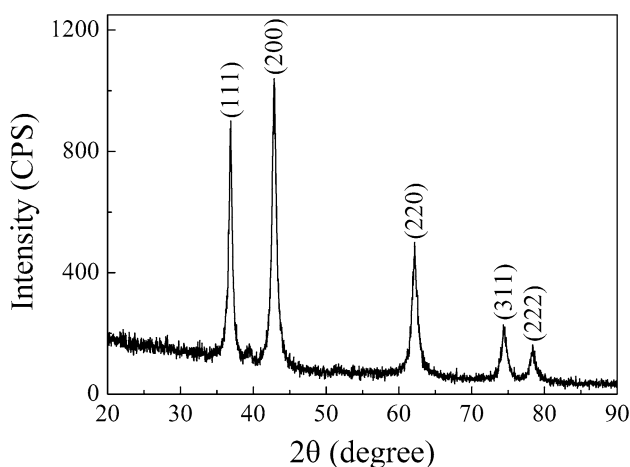


Fig. 1 XRD pattern of the TiN sample synthesized at 700 °C for 1 h

Table 1 Reference interplanar distances of the TiN phase in comparison with XRD result

Crystal plane	Interplanar distances d (Å)	
	JCPDS file no. 38-1420	XRD result
111	2.4492	2.4372
200	2.1207	2.1101
220	1.4997	1.4919
311	1.2789	1.2746
222	1.2245	1.2205

3.2 Morphologies

The morphology and crystal structure of the final TiN nanoparticles can be observed in Fig. 2. The HR-TEM image clearly shows the structural feature of the nanoparticles, as shown in Fig. 2a. It also can be observed that the TiN particles exist obvious aggregation with smaller grown nanoparticles, exhibiting a large surface area (will be discussed later). The spacing between adjacent lattice planes is measured to be 0.25 nm, corresponding to the (111) plane of TiN. However, these lattice fringes are in different orientations (Fig. 2b), indicating the polycrystalline nature of the TiN nanomaterial, which is consistent with the result of the selected area electron diffraction (SAED) pattern (inset in Fig. 2d) of the sample. The d -spacings from inside to outside sequentially at 2.37 , 2.04 , 1.49 and 1.21 Å can be indexed to the (111), (200), (220) and (311) planes of the cubic phase, corresponding to the XRD result.

3.3 XPS investigations

The XPS spectra of the final TiN sample are shown in Fig. 3. The full range XPS spectrum in Fig. 3a clearly shows that the TiN sample surface mainly consists of titanium, nitrogen, carbon and oxygen. In addition to the reference carbon, the oxygen peaks observed may be due to the incomplete oxide reaction. The Ti2p spectrum of TiN nanoparticles is also given in Fig. 3b, in which the deconvolution of the Ti2p peak shows two components: TiN (Ti2p $_{3/2}$: 454.9 eV, Ti2p $_{1/2}$: 460.5 eV) and TiO $_2$ (Ti2p $_{3/2}$: 458.5 eV, Ti2p $_{1/2}$: 464.1 eV) [31, 32]. Figure 3c shows the N1s bands of the TiN nanoparticles. The major N1s peak at 396.1 eV can be indexed to the typical nitrogen shifts of TiN component, while the other two peaks at 397.1 and 398.7 eV are attributed to N–Ti on the TiN surface or impurities [31]. The quantitative analysis of the elements at the sample surfaces is given in Table 2, using the elemental sensitivity factor method.

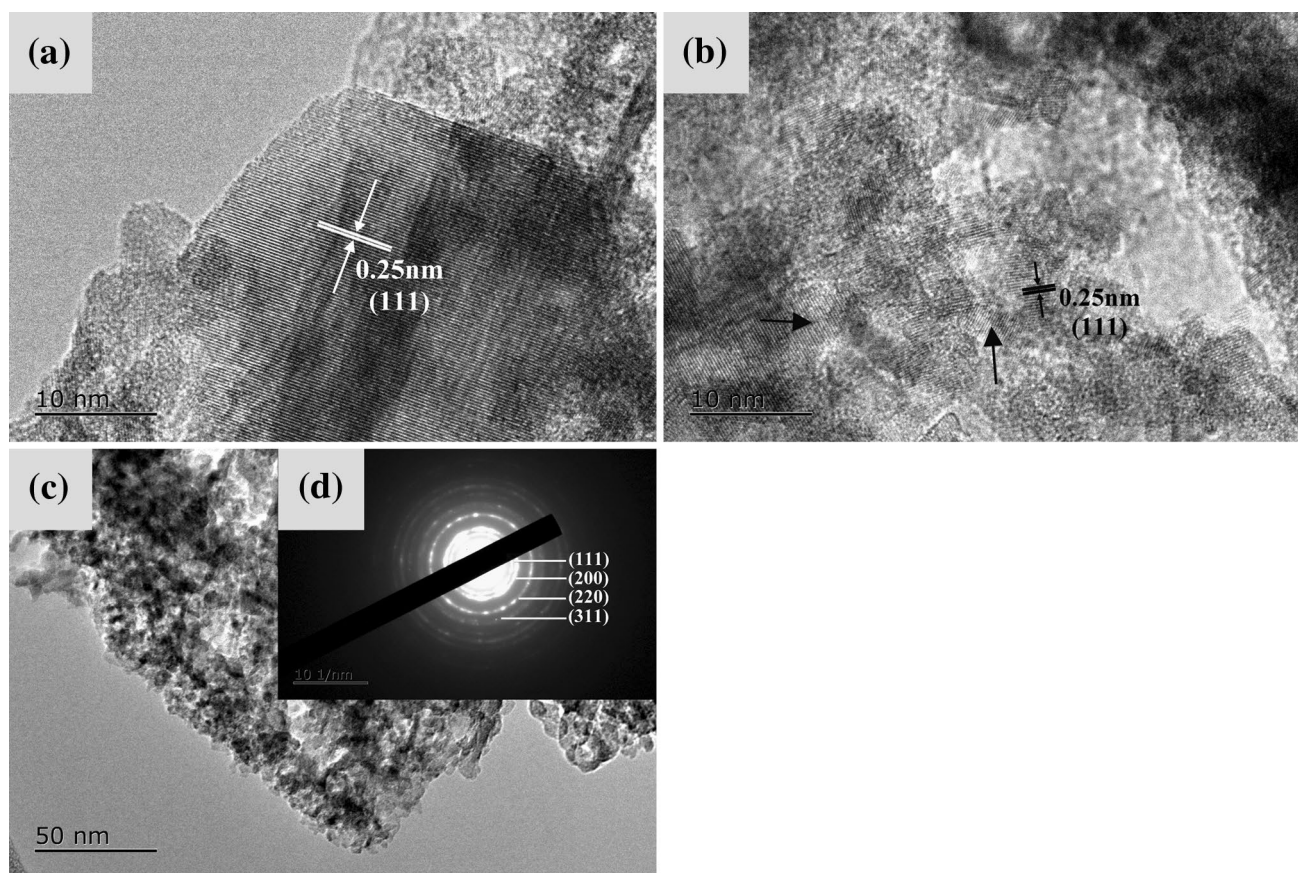


Fig. 2 TEM images of the TiN sample synthesized at 700 °C for 1 h: **a** and **b** HR-TEM image of the as-prepared TiN; **c** low-magnification TEM image of the as-prepared TiN; **d** SAED pattern obtained from (c)

3.4 BET surface area and pore size distribution

Figure 4 shows the N_2 adsorption–desorption isotherm and the corresponding pore size distribution curve of the TiN sample. The specimen is classified type-IV, which indicates the presence of mesopores [33]. The high N_2 adsorption values at the P/P_0 between 0.6 and 1.0, indicative of the existence of large mesopores, corresponding to the pore size distribution curve (inset of Fig. 4), showing a wide range of 1–30 nm with a peak pore diameter of ~3 nm. The BET surface area of the TiN nanoparticles is calculated to be 107.748 m^2/g .

3.5 Electrochemical performance

TiN served as working electrode directly, carbon rods as the counter electrode, a saturated calomel electrode (SCE) as reference electrode and tested in three-electrode system with 1 M Na_2SO_4 solution. The capacitance of TiN was studied by cyclic voltammetry (CV) method at different scan rates of 10, 20, 50, 100 and 200 mV/s. The

CV curves have a similar rectangular shape indicating the excellent conductivity of TiN (Fig. 5a). At the same time, the galvanostatic charge–discharge (GCD) curves are also showing the highly symmetry and exhibiting short voltage drop at current densities from 0.25 to 4 A/g (Fig. 5b). Therefore, we calculate the capacity of TiN used the following equation: [34]

$$C = I\Delta t / \Delta V$$

where C denotes the mass specific capacitance (F/g); Δt denotes the discharge time; I denotes the current density and ΔV denotes the potential window. The capacitance of TiN is 26.4 F/g at 0.25 A/g and 9.9 F/g at 4 A/g, respectively. Because of the excellent conductivity of TiN, the capacitance of TiN is remain 50% when the current density is aggrandize 16 times from 0.25 to 4 A/g. Figure 5d shows the Nyquist plots of the electrochemical impedance spectroscopy (EIS) for the TiN nanoparticles. The magnified spectrum in high frequency regions shows a low internal resistance (R_s) of 2.0 Ω for TiN nanoparticles (inset in Fig. 5d), implying the good conductivity of the sample.

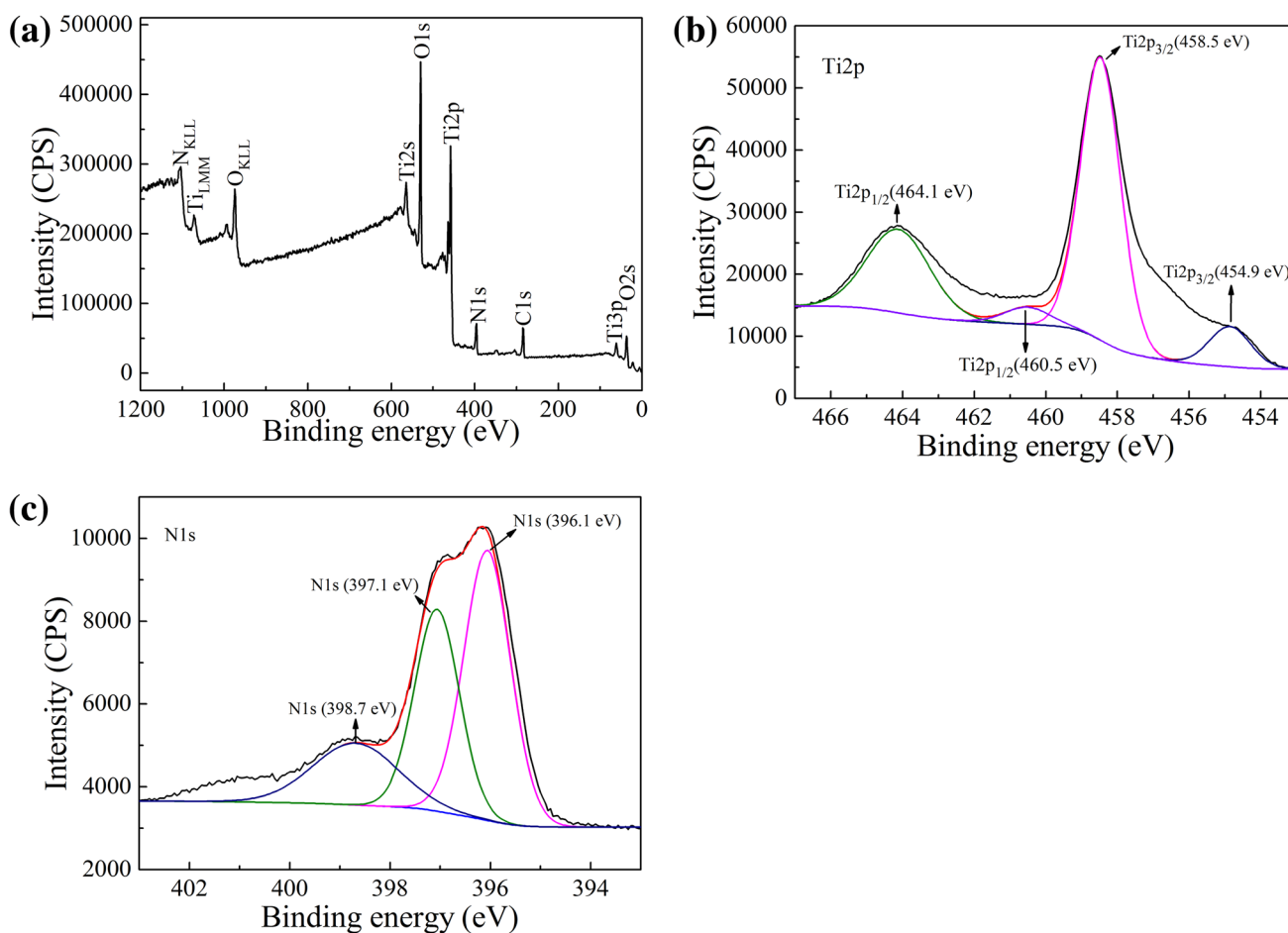


Fig. 3 XPS spectra of the TiN sample synthesized at 700 °C for 1 h: **a** Full XPS spectrum; **b** Ti2p spectrum; **c** N1s spectrum

Table 2 Elemental quantitative analysis using XPS for the TiN sample synthesized at 700 °C for 1 h

	FWHM (eV)	Raw area	RSF	Atomic conc. (%)
Ti2p	1.390	101233.5	2.001	20.16
N 1s	1.999	14516.4	0.477	12.27
O 1s	1.444	87226.3	0.780	44.12

The RSF is the relative sensitivity factor

3.6 Photoluminescence (PL) property

The PL technique has been widely used to study the optical and photochemical properties of semiconductor materials [35–37]. The PL spectrum of the TiN sample recorded at room temperature is shown in Fig. 6. The PL emission of the TiN nanoparticles, which was measured at 845 nm excitation wavelength, is composed of four prominent and high intense peaks centered at 279 (4.44), 420 (2.95), 561 (2.21) and 838 (1.48 eV) nm. The peaks centered at 420

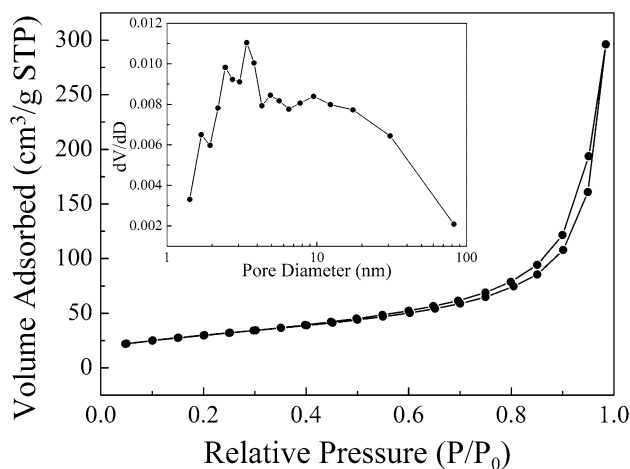


Fig. 4 Nitrogen adsorption–desorption isotherm and the corresponding pore-size distribution curve (inset) of the TiN sample synthesized at 700 °C for 1 h

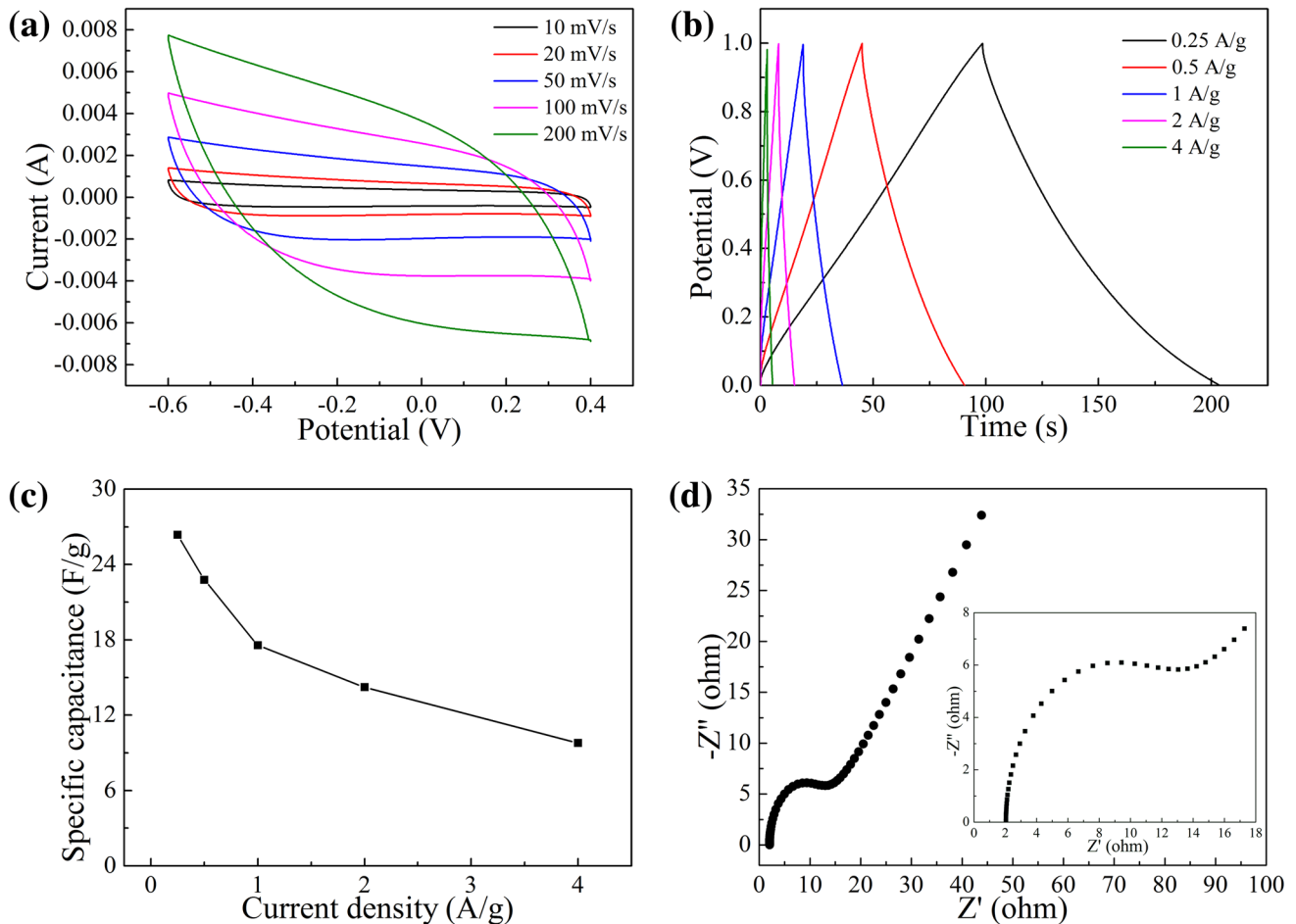


Fig. 5 Electrochemical performance of the TiN sample synthesized at 700 °C for 1 h: **a** CV curves at different scan rates; **b** GCD curves; **c** Specific capacitance at different current densities; **d** Nyquist plots

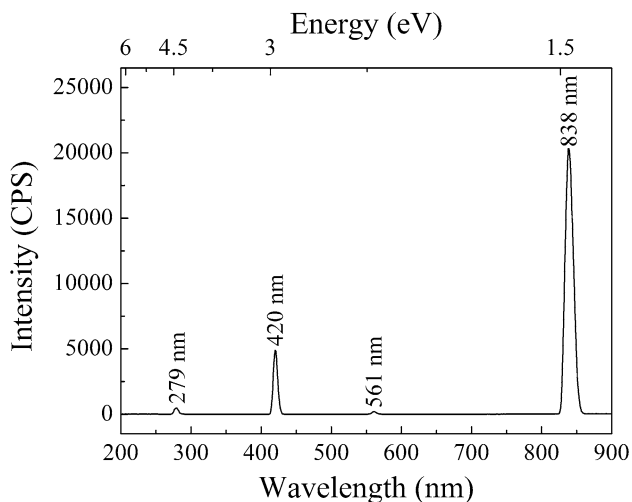


Fig. 6 Emission photoluminescence spectrum of the TiN sample synthesized at 700 °C for 1 h

and 561 nm are good evidences that the TiN nanoparticles could be applied as photoluminescence material.

4 Conclusions

In this work, TiN nanoparticles have been efficiently synthesized by molten-salt method in $\text{MgCl}_2\text{-NaCl}$ media at a low temperature of 700 °C for 1 h, using TiO_2 and Mg as raw materials in a N_2 atmosphere. It is found that the final TiN is a pure phase and highly crystalline, and has a high BET surface area (107.748 m^2/g). The specific capacitance of the TiN nanoparticles is 26.4 F/g at 0.25 A/g discharge current density and the internal resistance (R_s) is as low as 2.0 Ω. The photoluminescence emission spectrum is measured at an excitation wavelength of 854 nm and four prominent and high intense peaks centered at 279, 420, 561 and 838 nm are observed.

Acknowledgements The authors acknowledge financial support from the National Natural Science Foundation of China (Grant Nos. 51502215, 51574187 and 51602232).

References

- H.T. Liu, Z.H. Huang, J.T. Huang, J.Z. Yang, M.H. Fang, Y.G. Liu, X.W. Wu, Unique single-crystal TiN_{1+x} nano-rods: synthesis, electrical transportation, and electric field effect conductivity. *Mater. Des.* **111**, 541–547 (2016)
- R.K. Yang, C.S. Zhu, Q. Wei, Z. Du, Investigations on structural, elastic, thermodynamic and electronic properties of TiN, Ti_2N and Ti_3N_2 under high pressure by first-principles. *J. Phys. Chem. Solids* **98**, 10–19 (2016)
- V. Merie, M. Pustan, G. Negrea, C. Birleanu, Research on titanium nitride thin films deposited by reactive magnetron sputtering for MEMS applications. *Appl. Surf. Sci.* **358**, 525–532 (2015)
- K. Vasu, M.G. Krishna, K.A. Padmanabhan, Substrate-temperature dependent structure and composition variations in RF magnetron sputtered titanium nitride thin films. *Appl. Surf. Sci.* **257**(7), 3069–3074 (2011)
- N. Jiang, H.J. Zhang, S.N. Bao, Y.G. Shen, Z.F. Zhou, XPS study for reactively sputtered titanium nitride thin films deposited under different substrate bias. *Phys. Rev. B* **352**(1–4), 118–126 (2004)
- I.G. Morozov, O.V. Belousova, O.A. Belyakov, I.P. Parkin, S. Sathasivam, M.V. Kuznetsov, Titanium nitride room-temperature ferromagnetic nanoparticles. *J. Alloys Compd.* **675**, 266–276 (2016)
- Y.H. Xiao, G.H. Zhan, Z.G. Fu, Z.C. Pan, C.M. Xiao, S.K. Wu, C. Chen, G.H. Hu, Z.G. Wei, Robust non-carbon titanium nitride nanotubes supported Pt catalyst with enhanced catalytic activity and durability for methanol oxidation reaction. *Electrochim. Acta* **41**(28), 279–285 (2014)
- J. Tavares, S. Coulombe, J.L. Meunier, Synthesis of cubic-structured monocrystalline titanium nitride nanoparticles by means of a dual plasma process. *J. Phys. D* **42**(10), 102001–102004 (2009)
- D.Q. Yin, X.H. Peng, Y. Qin, Z.C. Wang, Template effect in TiN/AlN multilayered coatings from first principles. *Ceram. Int.* **41**(8), 10095–10101 (2015)
- U. Guler, S. Suslov, A.V. Kildishev, A. Boltasseva, V.M. Shalaev, Colloidal plasmonic titanium nitride nanoparticles: properties and applications. *Nanophotonics* **4**(1), 269–276 (2015)
- B. Bora, N. Aomoa, M. Kakati, H. Bhuyan, Studies on a supersonic thermal plasma expansion process for synthesis of titanium nitride nanoparticles. *Powder Technol.* **246**(5), 413–418 (2013)
- N. Mosavati, V.R. Chitturi, S.O. Salley, K.Y.S. Ng, Nanostructured titanium nitride as a novel cathode for high performance lithium/dissolved polysulfide batteries. *J. Power Sources* **321**, 87–93 (2016)
- Y.Z. Jin, Y. Liu, J.W. Ye, B.H. Li, Effect of carbon source on the carbothermal reduction nitridation for synthesis of (Ti, W, Mo, V) (C, N) nanocrystalline powders. *Int. J. Refract. Met. Hard Mater.* **29**(2), 268–272 (2011)
- W.B. He, B.L. Zhang, H.R. Zhuang, W.L. Li, Combustion synthesis of Si_3N_4 -TiN composite powders. *Ceram. Int.* **30**(8), 2211–2214 (2004)
- H.J. Zhang, F.L. Li, Q.L. Jia, Preparation of titanium nitride ultrafine powders by sol-gel and microwave carbothermal reduction nitridation methods. *Ceram. Int.* **35**(3), 1071–1075 (2009)
- U.A. Joshi, S.H. Chung, J.S. Lee, Low-temperature, solvent-free solid-state synthesis of single-crystalline titanium nitride nanorods with different aspect ratios. *J. Solid State Chem.* **178**(3), 755–760 (2005)
- K. Wokulska, Thermal expansion of whiskers of Ti(C, N) solid solutions. *J. Alloys Compd.* **264**(1–2), 223–227 (1998)
- M. Wang, M.H. Fang, X. Min, Z.H. Huang, C. Tang, Y.G. Liu, X.W. Wu, Molten salt synthesis of $\text{NaNb}_x\text{Ta}_{1-x}\text{O}_3$ perovskites with enhanced photocatalytic activity. *Chem. Phys. Lett.* **686**, 18–25 (2017)
- S.W. Zhang, Y. When, H.J. Zhang, Low temperature preparation of tungsten nanoparticles from molten salt. *Powder Technol.* **253**(2), 464–466 (2014)
- J.K. Ye, S.W. Zhang, W.E. Lee, Molten salt synthesis and characterization of SiC coated carbon black particles for refractory castable applications. *J. Eur. Ceram. Soc.* **33**(10), 2023–2029 (2013)
- J. Ding, H.X. Zhu, G.Q. Li, C.J. Deng, J. Li, Growth of SiC nanowires on wooden template surface using molten salt media. *Appl. Surf. Sci.* **320**, 620–626 (2014)
- J. Ding, C.J. Deng, W.J. Yuan, H.X. Zhu, J. Li, Preparation of porous TiC/C ceramics using wooden template in molten salt media. *Adv. Appl. Ceram.* **112**(3), 131–135 (2013)
- J. Ding, C.J. Deng, W.J. Yuan, H.X. Zhu, X.J. Zhang, Novel synthesis and characterization of silicon carbide nanowires on graphite flakes. *Ceram. Int.* **40**(3), 4001–4007 (2014)
- J. Ding, H.X. Zhu, C.J. Deng, G.Q. Li, K.L. Wang, J.P. Liu, Preparation and characterization of porous biomorphic SiC/C ceramic from molten salt. *Ceram. Int.* **41**(9), 11539–11545 (2015)
- J. Ding, C.J. Deng, H.X. Zhu, X.J. Zhang, D. Guo, Novel preparation of a porous composite insulating scaffold from forsterite and sodium carbonate media. *Int. J. Mater. Res.* **105**(11), 1140–1144 (2014)
- J. Ding, C.J. Deng, W.J. Yuan, H.X. Zhu, J. Li, The synthesis of titanium nitride whiskers on the surface of graphite by molten salt media. *Ceram. Int.* **39**(3), 2995–3000 (2013)
- J. Ding, H.X. Zhu, G.Q. Li, C.J. Deng, Z.N. Chai, Catalyst-assisted synthesis of α - Si_3N_4 in molten salt. *Ceram. Int.* **42**(2), 2892–2898 (2016)
- Z.N. Chai, J. Ding, C.J. Deng, H.X. Zhu, G.Q. Li, C. Yu, Ni-catalyzed synthesis of hexagonal plate-like alpha silicon nitride from nitridation of Si powder in molten salt media. *Adv. Powder Technol.* **27**(4), 1637–1644 (2016)
- X.Q. Kan, J. Ding, C. Yu, H.X. Zhu, C.J. Deng, G.Y. Li, Low-temperature fabrication of porous ZrC/C composite material from molten salts. *Ceram. Int.* **43**, 6377–6384 (2017)
- F.H. Alhassan, U. Rashid, M.S. Al-Qubaisi, A. Rasedee, Y.H. Taufiq-Yap, The effect of sulfate contents on the surface properties of iron-manganese doped sulfated zirconia catalysts. *Powder Technol.* **253**(2), 809–813 (2014)
- L.L. Lin, S.A. Starostin, Q. Wang, V. Hessel, An atmospheric pressure microplasma process for continuous synthesis of titanium nitride nanoparticles. *Chem. Eng. J.* **321**, 447–457 (2017)
- S. Oktay, Z. Kahraman, M. Urgan, K. Kazmanli, XPS investigations of tribolayers formed on TiN and (Ti, Re)N coatings. *Appl. Surf. Sci.* **328**(2), 255–261 (2015)
- Q. Li, H. Meng, P. Zhou, Y.Q. Zheng, J. Wang, J.G. Yu, J.R. Gong, $\text{Zn}_{1-x}\text{Cd}_x\text{S}$ solid solutions with controlled bandgap and enhanced visible-light photocatalytic H_2 -production activity. *ACS Catal.* **3**(5), 882–889 (2013)
- M.Y. Zhang, X.W. Ma, H. Bi, X.B. Zhao, C. Wang, J. Zhang, Y.S. Li, R.C. Che, Facile preparation of 3D hierarchical coaxial-cable-like Ni-CNTs@beta-(Ni, Co) binary hydroxides for supercapacitors with ultrahigh specific capacitance. *J. Colloid Interface Sci.* **502**, 33–43 (2017)

35. Z.B. Wu, F. Dong, W.R. Zhao, S. Guo, Visible light induced electron transfer process over nitrogen doped TiO₂ nanocrystals prepared by oxidation of titanium nitride. *J. Hazard. Mater.* **157**(1), 57–63 (2008)
36. L.Q. Jing, Y.C. Qu, B.Q. Wang, S.D. Li, B.J. Jiang, L.B. Yang, W. Fu, H.G. Fu, J.Z. Sun, Review of photoluminescence performance of nano-sized semiconductor materials and its relationships with photocatalytic activity. *Sol. Energy Mater. Sol. Cells* **90**(12), 1773–1787 (2006)
37. L.F. Ye, L. Zhao, F. Liang, X. He, W. Fang, H. Chen, S.W. Zhang, S.H. An, Facile synthesis of hexagonal boron nitride nanoplates via molten-salt-mediated magnesiothermic reduction. *Ceram. Int.* **41**(10), 14941–14948 (2015)